Journal of Energy and Power Engineering 12 (2018) 80-92
doi: 10.17265/1934-8975/2018.02.004

Impact of Thickness of Polymer Electrolyte Membrane on Temperature Distributions in Single Cell of Polymer Electrolyte Fuel Cell Operated at High Temperature

Akira Nishimura, Yusuke Sato, Masato Yoshimura, Satoru Kamiya and Masafumi Hirota

Division of Mechanical Engineering, Graduate School of Engineering, Mie University, Tsu-city, Mie 514-8507, Japan

Abstract: This study is to understand the impact of operating condition, especially initial operation temperature (T_{ini}) which is set in high temperature range, on the temperature profile of the interface between PEM (polymer electrolyte membrane) and catalyst layer at the cathode (i.e., the reaction surface) in a single PEFC (polymer electrolyte fuel cell). A 1D multi-plate heat transfer model based on the temperature data of separator measured using thermograph in a power generation experiment was developed to evaluate the reaction surface temperature (T_{react}). This study investigated the effects of T_{ini}, flow rate and relative humidity of supply gas as well as thickness of PEM on the temperature distribution on reaction surface. As a result, the impact of flow rate of supply gas on the temperature distribution is not significant irrespective of relative humidity conditions as well as PEM type. When operated at high temperature, the temperature distribution is relatively flat in the case of thicker PEM (Nafion 115), while T_{react} rises from the inlet to the outlet large and the temperature distribution is wide in the case of thin PEM (Nafion 211) irrespective of relative humidity condition. Since the water transfer through PEM in the case of Nafion 211 is better than Nafion 115 due to thin PEM, the power generation is promoted along the gas flow with the aid of humidification by water produced from electrochemical reaction.

Key words: PEFC, heat transfer model, temperature distribution, high temperature operation, thickness of PEM.

1. Introduction

PEFC (polymer electrolyte fuel cell) is an attractive and clean power generation technology. However, there are some barriers preventing the widespread use of PEFCs among industries and homes worldwide. Some of such barriers are the reduction in the power generation performance and life span caused by the uneven distributions of a mass concentration and temperature inside a single cell of PEFC. Localized rise of temperature caused by local heat generation and poor gas diffusion blocked by the condensed water were thought to be reasons for the uneven temperature distribution [1-3].

The temperature distribution inside a single cell of PEFC is crucial to the performance of PEFC. Uneven temperature distribution would cause degradations of PEM (polymer electrolyte membrane) and catalyst layer. Localized temperature rise would cause thermal decomposition of PEM. The PEM could also be broken by thermal stress caused by the uneven temperature distribution [2, 4]. Temperature distribution also influences the phase change of water. Water's behavior influences the performance of the PEM, gas flows in GDL (gas diffusion layer) and catalyst layer. Hence, it is important to understand the temperature distribution in single cell of PEFC in order to improve the power generation performance and realize the long life span, which is the aim of this study.

The current PEFC has Nafion membrane and is usually operated within the temperature range between 60 °C and 80 °C [5, 6]. It is desired that PEFC operating temperature could be increased to 90 °C for stationary applications during period from 2020 to 2025 in Japan (according to NEDO road map 2017 [7]). The PEFC operated at a higher operating

Corresponding author: Akira Nishimura, Ph.D., associate professor, research fields: heat transfer, fuel cell, photocatalyst and smart city.

temperature has following merits: (1) enhancement of electrochemical kinetics for both electrode reactions; (2) simplification in the cooling system due to increase in temperature gradient between the PEFC stack and coolant; (3) increase in tolerability of CO and allowing the PEFC to use lower quality reformed hydrogen [8]. To develop the PEFC system operated under high temperature condition, heat and mass transfer characteristics should be analyzed for power generation performance and system durability. The uneven temperature distribution would cause degradations of PEM and catalyst layer terribly under high temperature condition since it is easy to be dried.

Some researches reported that the characteristics of PEFC under high temperature range up to 200 °C [9-28]. However, most of them focused on characteristics of developed new material [9, 10, 13, 14, 18, 23, 24, 27], the power generation performance such as current density distribution, voltage change [12, 15-17, 21, 22, 25, 26], and durability [11]. Although a few research reported the temperature distribution in the single cell of PEFC operated at high temperature [19, 20, 28], the temperature near the interface between PEM and catalyst layer at cathode, which is named as a reaction surface in the present paper, was not investigated. Therefore, the heat and mass transfer characteristics of PEFC, which dominates the power generation performance, operated at high temperature are not clarified yet.

In the study conducted by Nishimura, et al. [29], the temperature distributions on separator's back of single cell of PEFC were measured by thermograph. Without disturbing heat and mass transfer due to installation of sensor, the temperature distribution under power generation conditions was measured accurately. Based on the measured data, the study tried to build an empirical model to predict the temperature distribution on reaction surface. According to a literature survey by the study, there was no previous study on estimating the temperature distribution on reaction surface from measured temperature data at separator's back. If the heat transfer model to predict the temperature distribution on reaction surface with the measured separator back's temperature would be developed, the temperature distribution on reaction surface could be easily estimated without difficult and complex temperature measurement.

In previous studies conducted by Nishimura, et al. [30-32], in order to estimate the temperature distribution inside single cell of PEFC, a 1D multi-plate heat transfer model using the temperature data of separator's back measured by thermograph under power generation was developed. Since the single cell of PEFC consists of some components having plate shapes such as PEM, catalyst layer, GDL and separator, the previous studies by Nishimura, et al. [30-32] proposed the heat transfer model assuming the heat transfer through multi-plates for these components of the cell. The reaction surface temperature (T_{react}) was calculated using the heat transfer model. This is a new approach to identify the heat transfer mechanism in single cell of PEFC by means of the data measured by the thermograph and the model developed. Comparing the results from this model [30-32] with the other heat transfer models [33-35], there were differences in terms of heat transfer calculations. However, the temperature gradients for the targeted regions under the similar operation conditions were almost the same [30]. Thus, it can be believed that, the heat transfer model proposed in the present study is reasonable.

The aim of the present paper is to predict the temperature distribution on the reaction surface using the heat transfer model under high temperature operation such as 90 °C condition, which is the target temperature for a stationary PEFC system during the duration from 2020 to 2025 according to NEDO road map [7] in Japan. This study investigates the effects of initial operation temperature (T_{ini}), flow rate, relative humidity of supply gas on temperature distribution on reaction surface. In addition, two types of PEM were evaluated to investigate the impact of its thickness on temperature distribution on reaction surface.

2. Calculation Procedures

2.1 1D Multi-plate Heat Transfer Model

Fig. 1 illustrates the multi-plate single cell PEFC module used in this study. In the module, the separator's back is the opposite side of surface contacting GDL. The separator's back surface temperatures $T_{surf,c}$ and $T_{surf,a}$ were measured using thermograph.

The heat transfer across the module is assumed to be in 1D direction only. In the module, the cell is divided into a gas channel and a rib part. In Fig. 1, the upper and lower parts represent rib part and channel part, respectively. For both parts, the heat transfer was assumed to be in the through-plane direction.

The reaction heat generated on reaction surface is transferred to the cathode and anode sides separately. Although the gas flowing through the gas channel from the inlet to the outlet of the cell carries away some heat, the amount of heat taken is less than 1% of the estimated reaction heat of approximately 20 W [30]. Therefore, the heat carried away by the gas flow was neglected in this model. Additionally, the mass flow rate of gas flowing through the gas channel is very small ranging from 10^{-8} to 10^{-6} kg/s, resulting that the thermal conduction of gas in the gas channel is assumed since the gas is thought to be static.

2.2 Heat Generation Rate by Reaction

The heat generation rate H_{react} as a reaction product is calculated as the follows:

$$H_{react} = E_i - W_E \quad (1)$$

where, E_i is the ideal (total) energy generation rate by the water formation from H_2 and O_2 based on higher heating value. W_E is the electric work generated by PEFC. E_i and W_E are expressed as follows:

$$E_i = m_{H2} \times q_{HHV} \quad (2)$$

$$W_E = I \times V \quad (3)$$

where, I is the load current obtained by the experiment. When using PEM of Nafion 115 and Nafion 211 which were investigated in this study, I was 20 A (= 0.80 A·cm^{-2}) and 18 A (= 0.72 A·cm^{-2}), respectively. V is the voltage obtained by the experiment. m_{H2} is the molar flow rate of supplied H_2, which is equal to the ideal reaction consumption rate of H_2 required for the

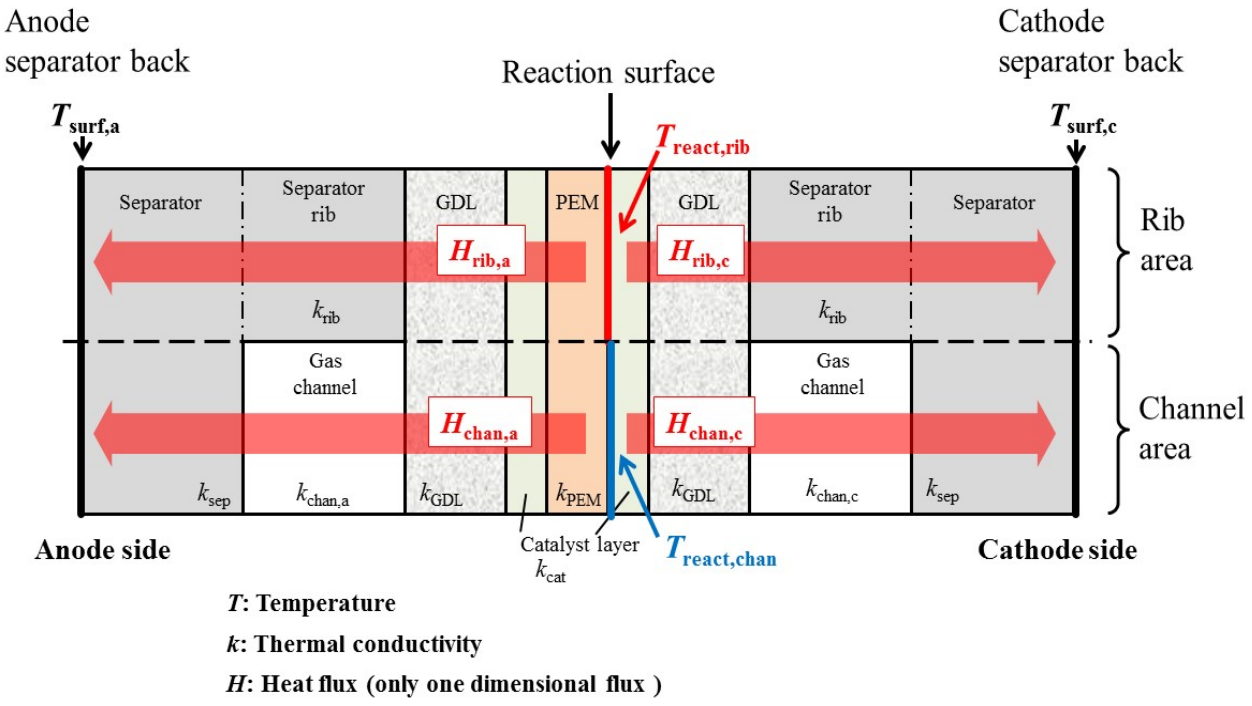

Fig. 1 1D multi-plate heat transfer module.

generation at 20 A, i.e., the stoichiometric ratio (s.r.) of 1.0. Here, s.r. is the ratio of the feed amount of H_2 or O_2 to that required to generate a current of 20 A. The flow rate of supply gas (H_2) at s.r. of 1.0 is defined as follows.

$$m_{H2} = I/nF \quad (4)$$

where, m_{H2} is the molar flow rate of supplied H_2 (mol·s^{-1}); n is the valence of ion (= 2 for H_2); F is the Faraday constant (= 96,500 C·mol^{-1}). m_{O2} which is the molar flow rate of supplied O_2 (mol·s^{-1}) and is calculated as follows:

$$H_2 + 1/2\ O_2 = H_2O \quad (5)$$

The actual s.r. of supply gas was confirmed, using the mass flow controller installed at the inlet of the single cell and the mass flow mater installed at the outlet of the cell in the power generation experiment [29].

2.3 Heat-Balance Equations for Calculating Reaction Surface Temperature

The heats transferred in the model proposed are expressed as Eqs. (6)-(10):

$$H_{rib,\,c} = K_{rib,\,c}\,A\,(T_{react,\,rib} - T_{surf,\,c})/2 \quad (6)$$

$$H_{chan,\,c} = K_{chan,\,c}\,A\,(T_{react,\,chan} - T_{surf,\,c})/2 \quad (7)$$

$$H_{rib,\,a} = K_{rib,\,a}\,A\,(T_{react,\,rib} - T_{surf,\,a})/2 \quad (8)$$

$$H_{chan,\,a} = K_{chan,\,a}\,A\,(T_{react,\,chan} - T_{surf,\,a})/2 \quad (9)$$

$$H_{react} = H_{rib,\,c} + H_{chan,\,c} + H_{rib,\,a} + H_{chan,\,a} \quad (10)$$

where, $H_{rib,\,c}$ is the heat flux to cathode side under rib (W); $K_{rib,\,c}$ is the overall heat transfer coefficient for cathode side under rib (W·m^{-2}·K^{-1}); A is the heat transfer area which is the active area of MEA, i.e., power generation area (= 0.0025 m^2); $T_{react,\,rib}$ is the reaction surface temperature under rib (K or °C); $T_{surf,\,c}$ is the separator's back surface temperature at cathode (K or °C); $H_{chan,\,c}$ is the heat flux to cathode side under channel (W); $K_{chan,\,c}$ is the overall heat transfer coefficient for cathode side under channel (W·m^{-2}·K^{-1}); $T_{react,\,chan}$ is the reaction surface temperature under channel (K or °C); $H_{rib,\,a}$ is the heat flux to anode side under rib (W); $K_{rib,\,a}$ is the overall heat transfer coefficient for anode side under rib (W·m^{-2}·K^{-1}); $T_{surf,\,a}$ is the separator's back temperature at anode (K or °C); $H_{chan,\,a}$ is the heat flux to anode side under channel (W); $K_{chan,\,a}$ is the overall heat transfer coefficient for anode side under channel (W·m^{-2}·K^{-1}). $K_{rib,\,c}$, $K_{chan,\,c}$, $K_{rib,\,a}$ and $K_{chan,\,a}$ are defined as follows:

$$1/K_{rib,\,c} = \delta_{cat}/k_{cat} + \delta_{GDL}/k_{GDL} + \delta_{rib}/k_{rib} + \delta_{sep}/k_{sep} \quad (11)$$

$$1/K_{chan,\,c} = \delta_{cat}/k_{cat} + \delta_{GDL}/k_{GDL} + \delta_{chan}/k_{chan,\,c} + \delta_{sep}/k_{sep} \quad (12)$$

$$1/K_{rib,\,a} = \delta_{PEM}/k_{PEM} + \delta_{cat}/k_{cat} + \delta_{GDL}/k_{GDL} + \delta_{rib}/k_{rib} + \delta_{sep}/k_{sep} \quad (13)$$

$$1/K_{chan,\,a} = \delta_{PEM}/k_{PEM} + \delta_{cat}/k_{cat} + \delta_{GDL}/k_{GDL} + \delta_{chan}/k_{chan,\,a} + \delta_{sep}/k_{sep} \quad (14)$$

where, δ_{cat} is the thickness of the catalyst layer (m); k_{cat} is the thermal conductivity of the catalyst layer (W·m^{-1}·K^{-1}); δ_{GDL} is the thickness of GDL (m); k_{GDL} is the thermal conductivity of GDL (W·m^{-1}·K^{-1}); δ_{rib} is the thickness of the separator rib (m); k_{rib} is the thermal conductivity of the separator rib (W·m^{-1}·K^{-1}); δ_{sep} is the thickness of the separator excluding rib part (m); k_{sep} is the thermal conductivity of the separator excluding rib part (W·m^{-1}·K^{-1}); δ_{chan} is the thickness of the channel of separator (m); k_{chan} is the thermal conductivity of the mixture gas in the channel of separator (W·m^{-1}·K^{-1}); δ_{PEM} is the thickness of PEM; k_{PEM} is the thermal conductivity of PEM.

Table 1 lists the specification of cell components used in the model. The materials of PEM, catalyst layer, GDL and separator are Nafion 115 or Nafion 211, compound of platinum and carbon, carbon paper and carbon graphite, respectively. The thickness values listed here are the same as those of the components used by previous studies [29, 36, 37].

In Table 1, the effective thermal conductivities of porous media k, are the values of the cell components used in the present experiment and in Refs. [29, 33]. Since the effective thermal conductivities given in Table 1 are obtained when the cell component pores are filled with air at room temperature, the corrected effective thermal conductivities are calculated for the cell component pores filled with H_2 or O_2 at 80 °C or

90 °C, which were the T_{ini} value assumed in this study. In this calculation, the thermal conductivities of each gas are from the Japan Society of Mechanical Engineers [38].

In order to solve Eqs. (6)-(9), the temperatures measured using the thermograph were substituted into these equations as $T_{surf,\ c}$ and $T_{surf,\ a}$. The operation conditions used for power generation in order to measure temperatures with thermograph are given in Table 2. Analysis using 1D multi-plate heat transfer is carried out by means of the data obtained under these conditions. The experimental procedure for measuring temperature during power generation has been explained in Refs. [29, 39].

In order to use the temperature data measured by thermograph in 1D multi-plate heat transfer model, the image of in-plane temperature distribution is divided into segments of 10 mm × 10 mm each, as shown in Fig. 2. Although the power generation area is 50 mm × 50 mm, the observation area is set to be 40 mm × 50 mm to prevent a gas leak through observation window in the experiments. The gas channel width and the rib width of investigated separator are 1.0 mm and the number of gas channel is 5. The segment includes the area consisting of five pairs of rib and gas channel. The average temperature in each segment at anode and cathode was used for the separator's back temperature in 1D multi-plate heat transfer model. The segment is named A to T along the gas flow direction as shown in Fig. 2.

Regarding segments A and T, the insulators covering the gas pipes interfere with the thermograph measurement in some area of the segment as it can be seen in Fig. 2. In this study, the effective temperature of segments A and T were obtained by removing the temperature data that were interfered by the insulator from the total temperature data in each segment. In the heat transfer analysis, it was assumed that $T_{surf,\ c}$ on the

Table 1 Specification of cell components.

Parts	Size	Characteristics	Porosity (-)	Effective thermal conductivity (W/m·K)
PEM	50.0 mm × 50.0 mm × 0.13 mm (Nafion 115) or 50.0 mm × 50.0 mm × 0.025 mm (Nafion 211)	Nafion 115 or Nafion 211 (produced by Du Pont Corp.)	0.15	0.195
Catalyst layer	50.0 mm × 50.0 mm × 0.01 mm (attached with PEM)	Pt/C (20 wt% Pt loading)	0.78	0.27
Gas diffusion layer (GDL)	50.0 mm × 50.0 mm × 0.17 mm	Carbon paper (TGP-H-060 produced by Toray Corp.)	0.78	1.7
Separator	75.4 mm × 75.4 mm × 2.00 mm (thickness of rib part: 1.00 mm) (gas supply area: 50.0 mm×50.0 mm)	Carbon graphite, serpentine	0.28	25

Table 2 Operating conditions of power generation for temperature measurement by thermograph.

Initial temperature of cell (°C)	80, 90	
Load current of cell (A) (Current density of cell ($A \cdot cm^{-2}$))	18 (Nafion 211), 20 (Nafion 115) (0.72, 0.80)	
Supply gas condition		
	Anode	Cathode
Gas type	H_2	O_2
Temperature of supply gas at inlet (°C)	80, 90	80, 90
Relative humidity of supply gas (% RH)	40, 80	40, 80
Pressure of supply gas at inlet (absolute) (MPa)	0.4	0.4
Flow rate of supply gas at inlet ($NL \cdot min^{-1}$) (Stoichiometric ratio (-))	0.210 (1.5), 0.280 (2.0), 0.420 (3.0)	0.105 (1.5), 0.140 (2.0), 0.210 (3.0)

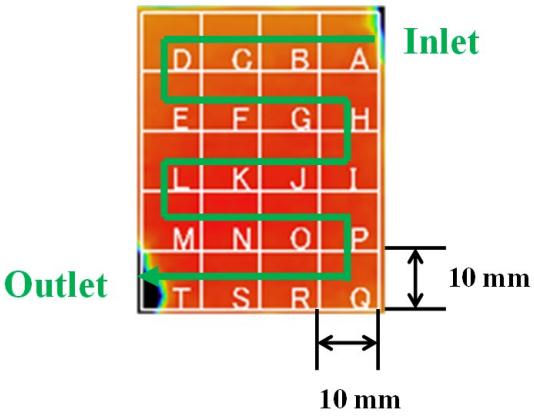

Fig. 2 Segment display of in-plane temperature distribution measured by thermograph.

rib side was equal to $T_{surf,\,c}$ on the channel side as well as $T_{surf,\,a}$ because the difference between them could not be recognized by the measured data.

Considering the above described assumptions and Eqs. (6)-(14), the reaction surface temperature T_{react} is expressed as follows:

$$T_{react} = T_{react,\,rib} = T_{react,\,chan} = \{2H_{react}/A + (K_{rib,\,c} + K_{chan,\,c})/T_{surf,\,c} + (K_{rib,\,a} + K_{chan,\,a})T_{surf,\,a}\}/(K_{rib,\,c} + K_{chan,\,c} + K_{rib,\,a} + K_{chan,\,a}) \quad (15)$$

3. Results and Discussion

3.1 Impact of Stoichiometric Ratio of Supply Gas on Temperature Distribution

Figs. 3 and 4 show the impact of s.r. of supply gas on temperature distribution on reaction surface simulated by the proposed heat transfer model for Nafion 115 and Nafion 212, respectively. The relative humidity of supply gases are 80% RH at the anode and 80% RH at the cathode (A80% RH, C80% RH), 80% RH at the anode and 40% RH at the cathode (A80% RH, C40% RH), and 40% RH at the anode and 80% RH at the cathode (A40% RH, C80% RH). The s.r. of supply gases are 1.5, 2.0 and 3.0. The results at T_{ini} = 90 °C are shown in these figures.

From these figures, it is observed that $T_{react} - T_{ini}$ increases along the gas flow from the inlet to the outlet gradually. Since the PEM is hydrated by the water produced by electrochemical reaction and the humidified gas flows through to the outlet, the power generation is promoted along the gas flow. In addition, it can be seen that the impact of flow rate of supply gas on the temperature distribution is not significant irrespective of relative humidity conditions as well as thickness of PEM. Since the gas supply is sufficient for power generation even s.r. = 1.5, it can be thought that the impact of flow rate of supply gas on the

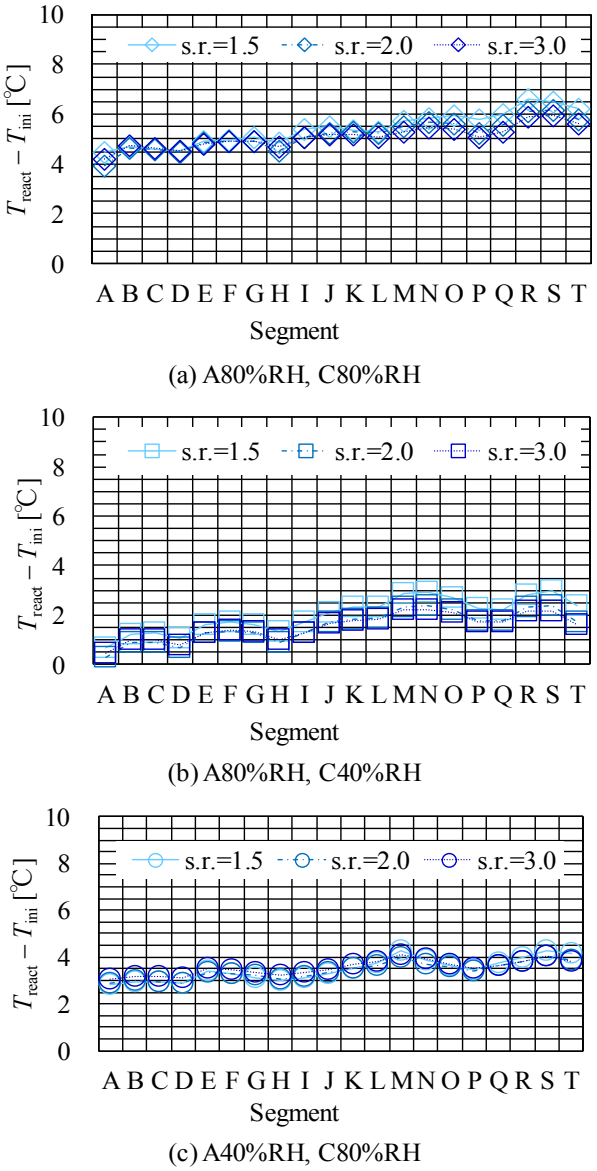

Fig. 3 Effect of stoichiometric ratio of supply gas on T_{react} for different relative humidity conditions at T_{ini} = 90 °C using Nafion 115.

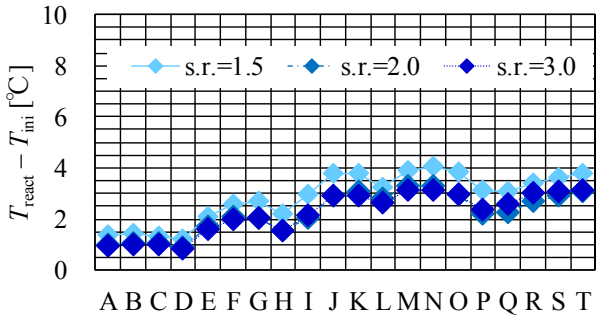

(a) A80%RH, C80%RH

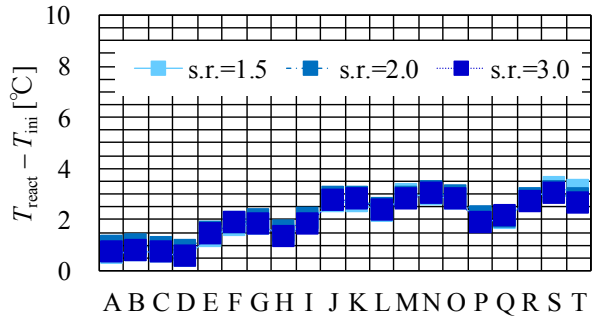

(b) A80%RH, C40%RH

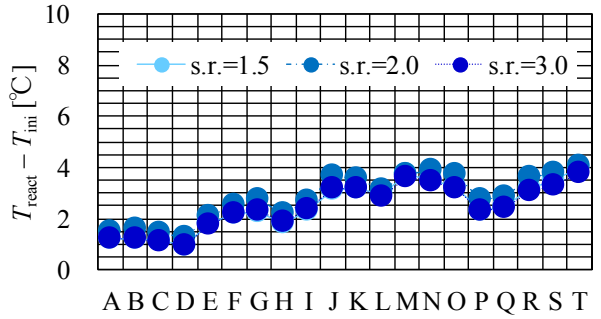

(c) A40%RH, C80%RH

Fig. 4 Effect of stoichiometric ratio of supply gas on T_{react} for different relative humidity conditions at T_{ini} = 90 °C using Nafion 211.

temperature distribution is not significant. Table 3 lists the power generation characteristics obtained by experiment in this study. From this table, the impact of flow rate of supply gas on the power generation performance is a little irrespective of relative humidity condition as well as T_{ini}. Therefore, the results for s.r. = 2.0 are shown about the following investigations in this paper since they can represent the characteristics of different stoichiometric ratios.

Table 3 Comparison of power generation performance obtained by power generation experiment among different operating conditions.

PEM	T_{ini} (°C)	Relative humidity of supply gas (% RH)	Flow rate of supply gas (s.r.)	Current (A), Voltage (V)
Nafion 115	80	A80% RH, C80% RH	1.5	20, 0.47
			2.0	20, 0.48
			3.0	20, 0.47
		A80% RH, C40% RH	1.5	20, 0.43
			2.0	20, 0.45
			3.0	20, 0.42
		A40% RH, C80% RH	1.5	20, 0.44
			2.0	20, 0.43
			3.0	20, 0.42
	90	A80% RH, C80% RH	1.5	20, 0.49
			2.0	20, 0.50
			3.0	20, 0.49
		A80% RH, C40% RH	1.5	20, 0.43
			2.0	20, 0.43
			3.0	20, 0.43
		A40% RH, C80% RH	1.5	20, 0.38
			2.0	20, 0.37
			3.0	20, 0.35
Nafion 211	80	A80% RH, C80% RH	1.5	18, 0.32
			2.0	18, 0.34
			3.0	18, 0.36
		A80% RH, C40% RH	1.5	18, 0.31
			2.0	18, 0.32
			3.0	18, 0.32
		A40% RH, C80% RH	1.5	18, 0.31
			2.0	18, 0.33
			3.0	18, 0.32
	90	A80% RH, C80% RH	1.5	18, 0.21
			2.0	18, 0.25
			3.0	18, 0.29
		A80% RH, C40% RH	1.5	18, 0.25
			2.0	18, 0.25
			3.0	18, 0.25
		A40% RH, C80% RH	1.5	18, 0.26
			2.0	18, 0.28
			3.0	18, 0.27

3.2 Impact of Initial Temperature of Cell on Temperature Distribution

Figs. 5-7 show the impact of T_{ini} on temperature distribution on reaction surface of Nafion 115 for several relative humidity conditions (A80% RH, C80% RH; A80% RH, C40% RH; A40% RH, C80%

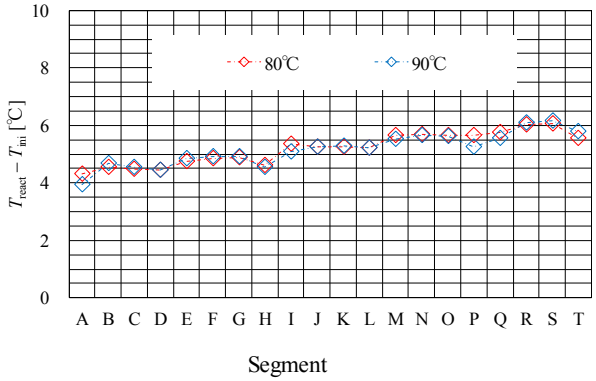

Fig. 5 Effect of T_{ini} on T_{react} for A80% RH, C80% RH using Nafion 115.

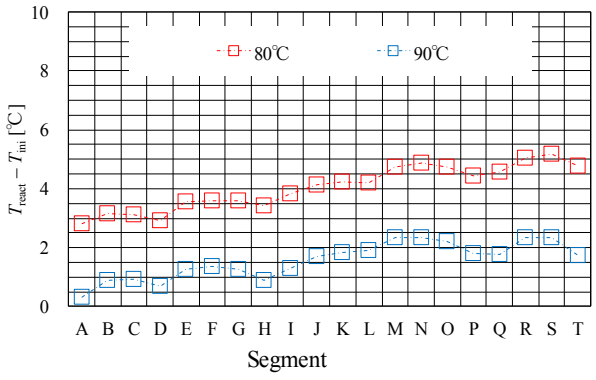

Fig. 6 Effect of T_{ini} on T_{react} for A80% RH, C40% RH using Nafion 115.

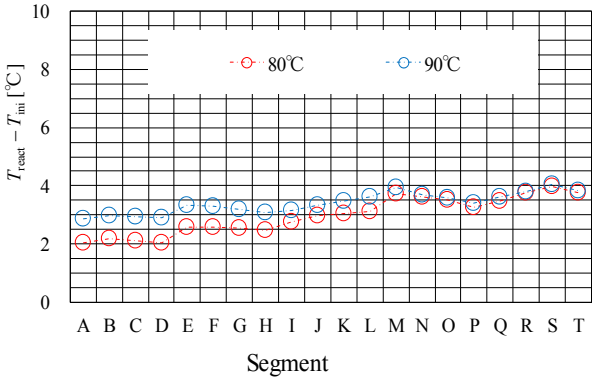

Fig. 7 Effect of T_{ini} on T_{react} for A40% RH, C80% RH using Nafion 115.

RH), respectively. The results for s.r. = 2.0 are shown in these figures.

It can be seen form Fig. 5 that the impact of T_{ini} on temperature distribution is not observed for A80% RH, C80% RH. Even T_{ini} = 90 °C which is easy to dry, temperature distribution is not affected by T_{ini} under the condition that the anode and the cathode are fully humidified. On the other hand, according to Fig. 6, $T_{react} - T_{ini}$ at T_{ini} = 90 °C is lower compared to that at T_{ini} = 80 °C under the condition of A80% RH, C40% RH. Since T_{ini} = 90 °C is dry condition and the relative humidity of the cathode is low, the proton conductivity of PEM and the reactivity of catalyst at the cathode are reduced. Therefore, the amount of liquid water which is produced by electrochemical reaction mainly is small, resulting that $T_{react} - T_{ini}$ is lower due to the decrease in the condensation heat of water. According to Fig. 7, there is the gap of $T_{react} - T_{ini}$ between T_{ini} = 80 °C and T_{ini} = 90 °C near the inlet. In other words, $T_{react} - T_{ini}$ at T_{ini} = 80 °C increases from the inlet to the outlet larger compared to that at T_{ini} = 90 °C. Since T_{ini} = 80 °C is more wet condition compared to T_{ini} = 90 °C and the condition of A40% RH, C80% RH causes back diffusion of water from the cathode to the anode easily, the power generation performance would be promoted. It can be also confirmed from Table 3 that the power generation performance for A40% RH, C80% RH at T_{ini} = 80 °C is better than that for A40% RH, C80% RH at T_{ini} = 90 °C.

Figs. 8-10 show the impact of T_{ini} on temperature distribution on reaction surface of Nafion 211 for several relative humidity conditions (A80% RH, C80% RH; A80% RH, C40% RH; A40% RH, C80% RH), respectively. The results for s.r. = 2.0 are shown in these figures. According to Figs. 8-10, it can be seen that temperature distribution is not affected by T_{ini} as well as relative humidity conditions though there is a little gap of $T_{react} - T_{ini}$ between T_{ini} = 80 °C and T_{ini} = 90 °C near the inlet. Since the water transfer through PEM is good for thin PEM [40], PEM is well humidified even high T_{ini} as well as low relative humidity condition. Therefore, the difference of $T_{react} - T_{ini}$ between T_{ini} = 80 °C and T_{ini} = 90 °C for each relative humidity conditions is small. The reason why there is a little gap of $T_{react} - T_{ini}$ between T_{ini} = 80 °C

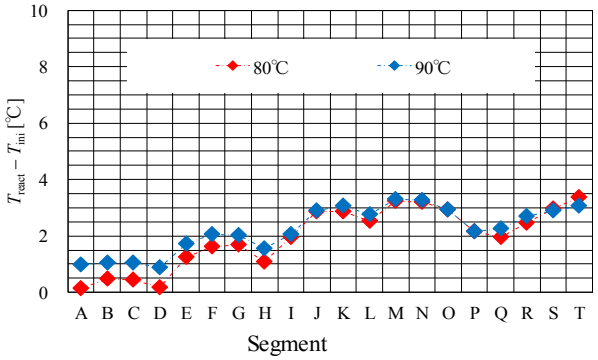

Fig. 8 Effect of T_{ini} on T_{react} for A80% RH, C80% RH using Nafion 211.

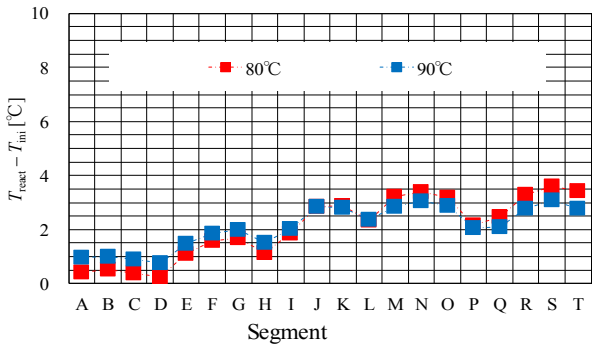

Fig. 9 Effect of T_{ini} on T_{react} for A80% RH, C40% RH using Nafion 211.

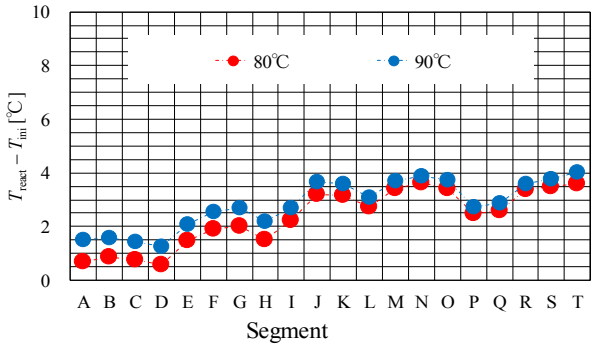

Fig. 10 Effect of T_{ini} on T_{react} for A40% RH, C80% RH using Nafion 211.

and T_{ini} = 90 °C near the inlet, i.e., $T_{react} - T_{ini}$ at T_{ini} = 80 °C increases from the inlet to the outlet larger compared to that at T_{ini} = 90 °C, is that T_{ini} = 80 °C is more wet condition compared to T_{ini} = 90 °C. Since the power generation performance would be promoted along the gas flow, the temperature rises from the inlet to the outlet at T_{ini} = 80 °C.

3.3 Impact of Thickness of PEM on Temperature Distribution

Figs. 11-13 show the impact of thickness of PEM on temperature distribution on reaction surface at T_{ini} = 90 °C for several relative humidity conditions (A80% RH, C80% RH; A80% RH, C40% RH; A40% RH, C80% RH), respectively. The results for s.r. = 2.0 are shown in these figures. According to Figs. 11-13, the temperature distribution is relatively flat in the case of Nafion 115. Since the water transfer is not good due to thick PEM, the humidification by the water generated from electrochemical reaction along the gas flow is small. Therefore, the temperature increase due to the condensation heat of water is a little. However, the condition of A80% RH, C80% RH is fully humidified, resulting that $T_{react} - T_{ini}$ is larger as shown in Fig. 11. On the other hand, $T_{react} - T_{ini}$ rises from the inlet to the outlet large and the temperature distribution is wide in the case of Nafion 211 irrespective of relative humidity condition. Since the water transfer through PEM is better than Nafion 115 due to thin PEM [40], the supplied gas is humidified by water produced from electrochemical reaction. Therefore, the power generation is promoted along the gas flow, resulting that the temperature rises from the inlet to the outlet.

From the investigation by this study, the temperature distribution on reaction surface under high temperature operation is different between two types of PEM whose thickness are different. Nafion 115 which is thicker PEM is affected by T_{ini} and relative humidity condition more significantly than Nafion 211. It can be alleged that Nafion 211 can save the energy and cost for pre-humidification since the same power generation performance, and heat and mass transfer characteristics are obtained under low relative humidity condition. Though the water transfer performance of Nafion 211 is better than that of Nafion 115, the power generation performance of Nafion 211 is worse than that of Nafion 115 according to Table 3. It is considered that the wide temperature

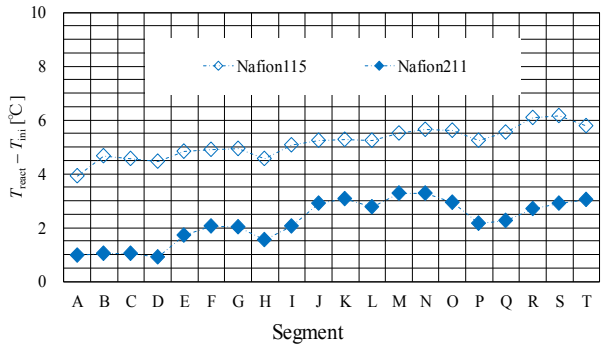

Fig. 11 Effect of PEM thickness on T_{react} for A80% RH, C80% RH.

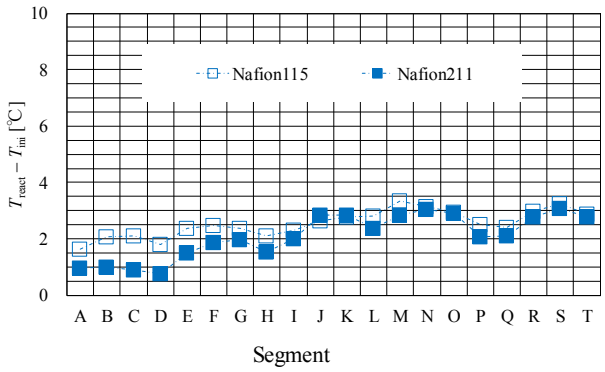

Fig. 12 Effect of PEM thickness on T_{react} for A80% RH, C40% RH.

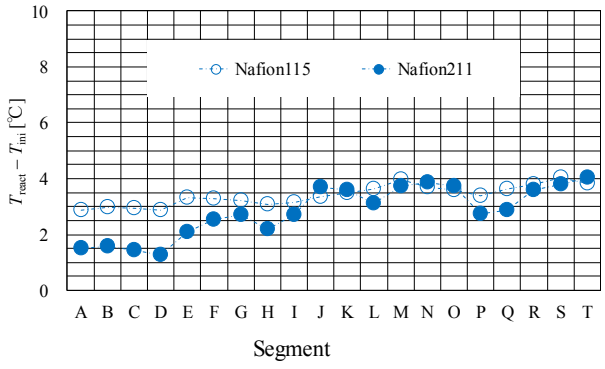

Fig. 13 Effect of PEM thickness on T_{react} for A40% RH, C80% RH.

distribution prevents Nafion 211 from conducting the power generation sufficiently. The power generation performance is better when the in-plane temperature distribution in the single cell is even [41]. Therefore, there are two key points to obtain the high power generation performance, i.e., keeping a good humidification through reaction surface and an even in-plane temperature distribution. To realize them simultaneously, it can be proposed that the water discharged from the outlet of the cell reuses in the cell by recirculation pipe line. It is promising that the temperature elevation on reaction surface is prevented by the improvement of power generation performance with the additional water management system providing the effective energy conversion to electricity.

4. Conclusions

The temperature distribution on reaction surface was calculated by the 1D multi-plate heat transfer model proposed by this study under high temperature operation such as 90 °C condition. In addition, the impacts of T_{ini}, flow rate, relative humidity of supply gas and thickness of PEM on the temperature distribution on reaction surface have been also investigated. From the investigation of this study, the following conclusions have been obtained:

(1) $T_{react} - T_{ini}$ increases along the gas flow from the inlet to the outlet gradually due to humidification by the water produced from electrochemical reaction though it is relatively flat for Nafion 115;

(2) The impact of flow rate of supply gas on the temperature distribution is not significant irrespective of relative humidity conditions as well as PEM type due to the sufficient gas supply;

(3) As to Nafion 115, the impact of T_{ini} on temperature distribution is not observed for A80% RH, C80% RH. However, the impact of T_{ini} on temperature distribution is observed for A80% RH, C40% RH and A40% RH, C80% RH. $T_{react} - T_{ini}$ at T_{ini} = 90 °C is lower compared to that at T_{ini} = 80 °C under the condition of A80% RH, C40% RH. $T_{react} - T_{ini}$ at T_{ini} = 80 °C increases from the inlet to the outlet larger compared to that at T_{ini} = 90 °C under the condition of A40% RH, C80% RH;

(4) As to Nafion 211, temperature distribution is not affected by T_{ini} as well as relative humidity conditions though there is a little gap of $T_{react} - T_{ini}$ between T_{ini} =

80 °C and T_{ini} = 90 °C near the inlet;

(5) Compared to Nafion 115, $T_{react} - T_{ini}$ rises from the inlet to the outlet large and the temperature distribution is wide in the case of Nafion 211 irrespective of relative humidity condition. Since the water transfer through PEM in the case of Nafion 211 is better than that in the case of Nafion 115 due to thin PEM, the power generation is promoted along the gas flow with the aid of humidification by water produced from electrochemical reaction;

(6) Though the water transfer performance of Nafion 211 is better, it is believed that the wide temperature distribution prevents Nafion 211 from conducting the power generation sufficiently.

Acknowledgments

This work was supported by Mie Prefecture Industrial Research Institute as well as Mie Industry and Enterprise Support Center. The authors acknowledge their great contribution.

References

[1] Weber, A. Z., Darling, R. M., and Newman, J. 2004. "Modeling Two-Phase Behavior in PEFCs." *Journal of Electrochemical Society* 151 (10): A1715-27.

[2] Wang, M., Guo, H., and Ma, C. 2006. "Temperature Distribution on the MEA Surface of a PEMFC with Serpentine Channel Flow Bed." *Journal of Power Sources* 157 (1): 181-7.

[3] Ito, K. 2008. "Temperature Distribution Measurement in Through-Plane Direction for PEFC." *Japan Society of Mechanical Engineers* 111 (1079): 42-4.

[4] Tsuji, K. 2008. "Domestic Fuel Cell Co-generation System Entering Real Commercial Stage." *Hydrogen Energy System* 33 (3): 93-6.

[5] Zhang, G., and Kandlikar, S. G. 2012. "A Critical Review of Cooling Technique in Proton Exchange Membrane Fuel Cell Stacks." *International Journal of Hydrogen Energy* 37 (February): 2412-29.

[6] Agbossou, K., Kolhe, M., Hamelin, J., and Bose, T. K. 2004. "Performance of a Stand-Alone Renewable Energy System Based on Energy Storage as Hydrogen." *IEEE Transactions on Energy Conversion* 19 (October): 633-40.

[7] NEDO (New Energy and Industry Technology Development Organization). 2017. "NEDO Road Map of Fuel Cell and Hydrogen Technology Development." Department of Fuel Cell and Hydrogen Technology. Accessed on March 6, 2018. http://www.nedo.go.jp/content/100871973.pdf.

[8] Li, Q., He, R., Jensen, J. O., and Bjerrum, N. J. 2003. "Approaches and Recent Development Polymer Electrolyte Membrane for Fuel Cells Operating above 100 °C." *Chemical of Materials* 15 (26): 4896-915.

[9] Zhang, Q., Ling, Y., Cai, W., Yu, X. and Yang, Z. 2017. "High Performance and Durability of Polymer-Coated Pt Electrocatalyst Supported on Oxidized Multi-walled in High-Temperature Polymer Electrolyte Fuel Cells." *International Journal of Hydrogen Energy* 42: 16714-21.

[10] Quartarone, E., Angioni, S., and Mustarelli, P. 2017. "Polymer and Composite Membranes for Proton-Conducting, High-Temperature Fuel Cells: A Critical Review." *Materials* 10 (687): 1-17.

[11] Thomas, S., Vang, J. R., Araya, S. S., and Kar, S. K. 2017. "Experimental Study to Distinguish the Effects of Methanol Slip and Water Vapour on a High Temperature PEM Fuel Cell at Different Operating Conditions." *Applied Energy* 192: 422-36.

[12] Rasheed, R. K. A., Liao, Q., Caizhi, Z., and Chan, S. H. 2017. "A Review on Modeling of High Temperature Proton Exchange Membrane Fuel Cells (HT-PEMFCs)." *International Journal of Hydrogen Energy* 42: 3142-65.

[13] Rosli, R. E., Sulong, A. B., Daud, W. A. R., Zulkifley, M. A., Husaini, T., Rosli, M. I., Majlan, E. H., and Haque, M. M. 2017. "A Review of High-Temperature Proton Exchange Membrane Fuel Cell (HT-PEMFC) System." *International Journal of Hydrogen Energy* 42: 9293-314.

[14] Lee, D., Lim, J. W., and Lee, D. G. 2017. "Cathode/Anode Integrated Composite Bipolar Plate for High-Temperature PEMFC." *Composite Structures* 167: 144-51.

[15] Singdeo, D., Dey T., Gaikwad, S., Andreasen, S. J., and Ghosh, P. C. 2017. "A New Modified-Serpentine Flow Field for Application in High Temperature Polymer Electrolyte Fuel Cell." *Applied Energy* 195: 13-22.

[16] Lakshmi, R. B., Harikrishnan, N. P., and Juliet, A. V. 2017. "Comparative Analysis of 2D and 3D Model of a PEMFC in COSOL." *Applied Surface Science* 418: 99-102.

[17] Lee, C. Y., Chiang, Y. C., Weng, F. -B., Li, S. C., Wu, P. H., and Yueh, H. I. 2017. "Flexible Micro Temperature, Voltage and Current Sensors for Local Real-time Microscopic Diagnosis inside High Temperature Proton Exchange Membrane Fuel Cell Stack." *Renewable Energy* 108: 126-31.

[18] Haque, M. A., Sulong, A. B., Loh, K. S., Majlan, E. H., Husaini, T., and Rosli, R. E. 2017. "Acid Doped Polybenzimidazoles Based Membrane Electrode Assembly for High Temperature Proton Exchange Membrane Fuel Cell: A Review." *International Journal of Hydrogen Energy* 42: 9156-79.

[19] Rasheed, R. K. A., Zhang, C., and Chan, S. H. 2017. "Numerical Analysis of High-Temperature Proton Exchange Membrane Fuel Cells during Start-Up by Inlet Gas Heating and Applied Voltage." *International Journal of Hydrogen Energy* 42: 10390-406.

[20] Lee, C. Y., Weng, F. B., Kuo, Y. W., Tsai, C. H., Cheng, Y. T., Cheng, C. K., and Lin, J. T. 2016. "In-situ Measurement of High-Temperature Proton Exchange Membrane Fuel Cell Stack Using Flexible Five-in-One Micro-sensors." *Sensors* 16 (1731): 1-10.

[21] Kim, H. S., Jeon, S. W., Cha, D., and Kim, Y. 2016. "Numerical Analysis of a High-Temperature Proton Exchange Membrane Fuel Cell under Humidified Operation with Stepwise Reactant Supply." *International Journal of Hydrogen Energy* 41: 13657-65.

[22] Zhang, C., Yu, T., Yi, J., Liu, Z., Raj, K. A. R., Xia, L., Tu, Z., and Chan, S. H. 2016. "Investigation of Heating and Cooling in a Stand-Alone High Temperature PEM Fuel Cell System." *Energy Conversion and Management* 129: 36-42.

[23] Araya, S. S., Zhou, F., Liso, V., Sahlin, S. L., Vang, J. R., Thomas, S., Gao, X., Jeppesen, C., and Kar, S. K. 2016. "A Comprehensive Review of PBI-Based High Temperature PEM Fuel Cells." *International Journal of Hydrogen Energy* 41: 21310-21344.

[24] Reimer, U., Ehlert, J., Janssen, H., and Lehnert, W. 2016. "Water Distribution in High Temperature Polymer Electrolyte Fuel Cells." *International Journal of Hydrogen Energy* 41: 1837-45.

[25] Waller, M. G., Walluk, M. R., and Trabold, T. A. 2016. "Performance of High Temperature PEM Fuel Cell Materials. Part 1: Effects of Temperature, Pressure and Anode Dilution." *International Journal of Hydrogen Energy* 41: 2944-54.

[26] Caglayan, D. G., Sezgin, B., Devrim, Y., and Eroglu, I. 2016. "Three-Dimensional Modeling of a High Temperature Polymer Electrolyte Membrane Fuel Cell at Different Operation Temperatures." *International Journal of Hydrogen Energy* 41: 10060-70.

[27] Jheng, L. C., Chang, W. J. Y., Hsu, S. L. C. and Cheng, P. Y. 2016. "Durability of Symmetrically and Asymmetrically Porous Polybenzimidazole Membranes for High Temperature Proton Exchange Membrane Fuel Cells." *Journal of Power Sources* 323: 57-66.

[28] Rasheed, R. K. A., and Chan, S. H. 2016. "Analysis of Steady State Heating Configuration for High-Temperature Proton Exchange Membrane Fuel Cell Based on Multi-physical Numerical Modeling." *Electrochimica Acta* 222: 280-92.

[29] Nishimura, A., Shibuya, K., Morimoto, A., Tanaka, S., Hirota, M., Nakamura, Y., Kojima, M., Narita, M., and Hu, E. 2012. "Dominant Factor and Mechanism of Coupling Phenomena in Single Cell of Polymer Electrolyte Fuel Cell." *Applied Energy* 90 (1): 73-9.

[30] Nishimura, A., Iio, K., Baba, M., Yamauchi, T., Hirota, M., and Hu, E. 2014. "Modeling of Heat Transfer in Single Cell of Polymer Electrolyte Fuel Cell by Means of Temperature Data Measured by Thermograph." *Journal of Chemical Engineering of Japan* 47 (7): 521-9.

[31] Nishimura, A., Fukuoka, T., Baba, M., Hirota, M., and Hu, E. 2015. "Clarification on Temperature Distribution in Single Cell of Polymer Electrolyte Fuel Cell under Different Operation Conditions by Means of 1D Multi-plate Heat-Transfer Model." *Journal of Chemical Engineering of Japan* 48 (10): 862-71.

[32] Nishimura, A., Osada, K., Tsunoda, T., Yoshimura, M., Hirota, M., and Hu, E. 2016. "Analysis on Temperature Distributions in Single Cell of Polymer Electrolyte Fuel Cell When Operated in High Temperature Range." *Journal of Energy and Power Engineering* 10: 453-64.

[33] Khandelwal, M., and Mench, M. M. 2006. "Direct Measurement of Through-Plane Thermal Conductivity and Contact Resistance in Fuel Cell Materials." *Journal of Power Sources* 161 (2): 1106-15.

[34] Kawase, M., Inagaki, T., Kawashima, S., and Miura, K. 2009. "Effective Thermal Conductivity of Gas Diffusion Layer in Through-Plane Direction." *ECS Transactions* 25 (1): 1529-37.

[35] Jung, C. Y., Shim, H. S., Koo, S. M., Lee, S. H., and Yi, S. C. 2012. "Investigation of the Temperature Distribution in Proton Exchange Membrane Fuel Cell." *Applied Energy* 93 (May): 733-41.

[36] Hwang, S. S., Han, S. S., Lee, P. H., and Park, B. I. 2010. "Transient Performance Behavior of Proton Exchange Membrane Fuel Cell by Configuration of Membrane and Gas Diffusion Layer." *Journal of Thermal Science and Technology* 5 (1): 165-77.

[37] Wu, H., Berg, P., and Li, X. 2010. "Steady and Unsteady 3D Non-isothermal Modeling of PEM Fuel Cells with the Effect of Non-equilibrium Phase Transfer." *Applied Energy* 87 (9): 2778-84.

[38] The Japan Society of Mechanical Engineers. 1993. *JSME Heat Transfer Handbook*. Maruzen, Tokyo.

[39] Nishimura, A., Yoshimura, M., Kamiya, S., Hirota, M., and Hu, E. 2017. "Impact of Relative Humidity of Supply Gas on Temperature Distribution in Single Cell of Polymer Electrolyte Fuel Cell when Operated at High

Temperature." *Journal of Energy and Power Engineering* 11: 706-18.

[40] Springer, T. E., Zawodzinski, T. A., and Gottesfeld, S. 1991. "Polymer Electrolyte Fuel Cell Model." *Journal of Electrochemical Society* 138 (8): 2334-42.

[41] Nishimura, A., Yoshimura, M., Mahadi, A. H., Hirota, M., and Kolhe, M. L. 2016. "Impact of Operation Condition on Temperature Distribution in Single Cell of Polymer Electrolyte Fuel Cell Operated at Higher Temperature than Usual." *Mechanical Engineering Journal* 3 (5): 1-14.